J. Fluid Mech. (1997), *vol.* 344, *pp.* 245–269. Printed in the United Kingdom

Lubrication flows between spherical particles colliding in a compressible non-continuum gas

By ARVIND GOPINATH, SHING B. CHEN† AND DONALD L. KOCH

School of Chemical Engineering, Cornell University, Ithaca, NY 14853, USA

(Received 20 June 1996 and in revised form 1 April 1997)

The low-Reynolds-number collision and rebound of two rigid spheres moving in an ideal isothermal gas is studied in the lubrication limit. The spheres are non-Brownian in nature with radii much larger than the mean-free path of the molecules. The nature of the flow in the gap between the particles depends on the relative magnitudes of the minimum gap thickness, h'_o, the mean-free path of the bulk gas molecules, λ_o, and the gap thickness at which compressibility effects become important, h_c. Both the compressible nature of the gas and the non-continuum nature of the flow in the gap are included and their effects are studied separately and in combination. The relative importance of these two effects is characterized by a dimensionless number, $\alpha_o \equiv (h_c/\lambda_o)$. Incorporation of these effects in the governing equations leads to a partial differential equation for the pressure in the gap as a function of time and radial position. The dynamics of the collision depend on α_o, the particle Stokes number, St_o, and the initial particle separation, h'_o. While a continuum incompressible lubrication force applied at all separations would prevent particle contact, the inclusion of either non-continuum or compressible effects allows the particles to contact. The critical Stokes number for particles to make contact, St_1, is determined and is found to have the form $St_1 = 2\ [\ln(h'_o/l) + C(\alpha_o)]$, where $C(\alpha_o)$ is an $O(1)$ quantity and l is a characteristic length scale defined by $l \equiv h_c(1 + \alpha_o)/\alpha_o$. The total energy dissipated during the approach and rebound of two particles when $St_o \gg St_1$ is also determined in the event of perfectly elastic or inelastic solid-body collisions.

1. Introduction

This paper deals with the dynamics of the approach and rebound of two spherical rigid non-Brownian particles in a gas governed by the ideal gas law. Both the compressible and the non-continuum nature of the gas flow in the gap between the particles is taken into account. A dimensionless parameter, α_o, which characterizes the relative importance of the two effects is identified. The critical Stokes number for which the approaching particles just touch one another is determined as a function of α_o. We also present expressions for the energy dissipated in the collision due to viscous effects in the limit of large Stokes numbers. This study complements previous work by Sundararajakumar & Koch (1996) on the energy dissipation due to incompressible lubrication flows during aerodynamic interparticle collisions.

Collisions between airborne particles play an important role in phenomena such as

† Present address: Department of Chemical Engineering, National University of Singapore, Singapore 119260.

coalescence of drops (Hocking & Jonas 1970; Mason 1971; Brazier-Smith, Jennings & Latham 1972; Pruppacher & Klett 1978; Ochs & Beard 1985), scavenging of dust particles (Chang, Leong & Stukel 1987), aerosol coagulation (Spielman 1970; Friedlander 1977; Schmidt-Ott & Burtscher 1982; Alam 1987) and combustion. In addition, there are industrially important processes involving fluidized beds and pneumatic transport, where accurate models for the collision dynamics between particles and between particles and surfaces are required (Koch 1990). In these models, the macroscopic equations characterizing the particulate phase include terms representing the exchange of momentum and energy between particles in a collision. A knowledge of the dependence of these terms on the nature of the surrounding medium and on fluid–particle interactions is thus essential.

The relative motion of two particles in close proximity to one another under conditions of small Reynolds number is usually modelled using the standard lubrication theory (Leal 1992), which assumes that the fluid is incompressible and may be treated as a continuum. This approach however leads to results which do not conform to what is seen in practice. The standard lubrication resistance to the relative motion of two spheres along their line of centres is inversely proportional to the separation distance and this implies that spheres with finite kinetic energy never collide. Hence in calculations employing the continuum theory, a collision is assumed to have taken place when the particles come within a specified distance of each other. Such an approach is useful only if the computed collision efficiencies are relatively insensitive to the cut-off distance. It has been observed that this approximation leads to significant errors for particles or drops with radii larger than about 30 μm (Hocking & Jonas 1970; Jonas & Goldsmith 1972; Pruppacher & Klett 1978). In addition, the incompressible continuum theory does not allow for rebound and hence the sticking efficiency is assigned an arbitrary value. This *ad hoc* procedure often leads to erroneous values of the collision and coalescence rate. It should be noted that viscous forces could reduce or increase the coalescence rate depending on the inertia of the colliding particles. For small drops/particles the viscous resistance decreases the collision rate (and hence the coalescence rate). Viscous forces can prevent larger drops or particles from rebounding and thus increase the coalescence rate.

Many recent theoretical studies have focused attention on collisions between spheres separated by a thin film of viscous liquid. Davis, Serraysol & Hinch (1986) studied collisions of deformable and rigid spheres in a compressible liquid. They found that particles with sufficiently large inertia could rebound without coming into contact. They also observed that the deformation of the solid surfaces had a stronger influence on the collision process than did the compressibility of the liquid in the gap. Kytömaa & Schmid (1992) considered collisions between two equal-sized spheres in a weakly compressible liquid using a regular perturbation method. The effect of interparticle attraction has also been studied (Rogers & Davis 1990; Serayssol & Davis 1986) for both deformable and rigid particles colliding in a liquid.

However, collisions in a gas are very different from those occurring in a liquid. The dynamic pressure in the gap is not as high in a gas as it is in a liquid and as a result the particles do not deform significantly before solid-body contact is achieved. In addition, the density in a gas can change much more than in a liquid. This raises the possibility that the gas in the gap can be compressed with a smaller pressure rise than would be required to drive its viscous flow out of the gap. The flow will deviate significantly from incompressible flow when the pressure required to drive the gas out of the gap becomes comparable to the bulk pressure. Consider the case of a collision between two identical spheres moving towards each other with

equal speeds. Using the scaling of the pressure for incompressible lubrication flow, $p = O(\mu_o U_o a/h'^2)$, h' being the minimum gap thickness, we can obtain an estimate of the relevant length, h_c, at which compressibility effects become important. This is given by $h_c \equiv (2\mu_o U_o a/p_o)^{1/2}$. Here a is the radius of the spherical particle, U_o is a characteristic particle speed, μ_o is the bulk viscosity of the gas and p_o is the bulk pressure. When the particle separation is comparable to or smaller than h_c the use of incompressible theory in describing the collision process is not justified. Furthermore, when the gap between the particles becomes comparable to the mean free path of the molecules, λ_o, the description of the gas as a continuum breaks down. While non-continuum effects are usually unimportant for particle collisions in liquids, the mean free path of the gas molecules is about 0.1 μm under standard atmospheric conditions. When the separation between aerosol particles becomes comparable to or smaller than this value, the non-continuum effect has to be taken into account.

Thus we find that a complete description of collisions in a gas requires rederiving the governing equations to account for the compressible, non-continuum nature of the gas flow in the gap at small separations. Since compressibility and non-continuum effects may both be important, it is useful to define a new dimensionless variable, $\alpha_o \equiv (h_c/\lambda_o)$, denoting the relative importance of the two effects. This parameter increases with increasing particle radius and relative velocity. For particles of diameter 100 μm colliding with a relative velocity comparable to their terminal velocities, $\alpha_o \sim O(1)$.

Although effects of compressibility on collisions in a gas have not been studied previously, the problem of incompressible non-continuum flow has been considered in some previous investigations. Hocking (1973) incorporated the first effects of the discrete nature of the gas in an analysis of the lubrication flow between two spheres by using the Maxwell slip condition instead of the conventional no-slip condition at the particle surfaces. His studies showed that particles with sufficient inertia could come into contact in a finite time. Hocking used the slip approximation for arbitrary particle separations, even though it is valid only when the gap thickness is much greater than the mean free path, i.e. $h'/\lambda_o \gg 1$. The slip approximation was also used by Ying & Peters (1989) for calculating the resistivity functions for a two-sphere system and by Barnocky & Davis (1989) for studying the aerodynamic collision and rebound of slightly deformable spherical particles in the presence of interparticle forces. A rough approximation for non-continuum effects has also been included in a study of Brownian coagulation of aerosols. Alam (1987) studied Brownian coagulation using a resistivity function that was an interpolation between the continuum flow solution including hydrodynamic interactions and a free-molecule flow result excluding hydrodynamic interactions. Extensive discussions of previous work and of two-particle collision mechanisms incorporating non-continuum effects (to some extent) may be found in the books by Pruppacher & Klett (1978) and by Williams & Loyalka (1991).

More recently, Sundararajakumar & Koch (1996) studied the incompressible flow between colliding spheres when $(h'/\lambda_o) \sim O(1)$. Under conditions of small Mach number, $M \equiv (U_o/\bar{c}) \ll 1$, the flow in the small gap is governed by the linearized Boltzmann equation. Here $\bar{c}$ is the mean thermal speed of the bulk gas molecules. It was shown that the flow in the gap could be approximated locally as a Poiseuille flow between two flat plates, as is done in the case of continuum flow. This result was obtained by introducing the standard lubrication scalings into the Boltzmann equation. Thus, the pressure profile and the force could be derived by replacing the continuum Poiseuille flow result with the relationship given by Cercignani & Daneri (1963) for the flux caused by a pressure gradient in the non-continuum flow between two (locally) flat plates. The incompressible analysis is valid for moderately large

particles (diameter in the range 10–50 μm). For larger particles one must consider the compressible nature of the gas in the gap in addition to non-continuum effects as we have done in § 2 and § 3.

In this paper, we consider collisions between two identical rigid spheres moving with equal and opposite velocities in an isothermal strongly compressible gas governed by the ideal equation of state:

$$p' M_w = \rho' R T,$$

where M_w is an effective molecular weight. Only collisions in which the relative velocity is along the line of centres are considered. However, both the compressiblity of the gas and the discrete nature of the flow are taken into account. We assume that the molecules undergo diffuse reflection at the particle surfaces. Since the terminal velocities encountered are small, the Mach number is small. In addition, we only consider cases where $(\lambda_o/a) \ll 1$ and $(h_c/a) \ll 1$, so that there exists a gap thickness that is small enough for the lubrication analysis to hold but large enough to neglect compressible and non-continuum effects.

For typical aerosol particle collisions, the range of the van der Waals attractions is smaller than the length scale on which the majority of the viscous dissipation takes place. Thus, it is attractive to decouple the consideration of the gas flow and the interparticle forces. We will compute the change in relative velocity of two particles as they move from an initial separation that is within the lubrication regime but much larger than λ_o and h_c until they come into contact. Although interparticle forces are neglected in this study, our result could be coupled with a description of the adhesive energy between the particles (Dahneke 1973) to obtain a criterion for coagulation. In addition to computing the resistance to approach of two particles, we also consider particle rebound under assumptions of perfectly elastic solid-body collisions or collisions that can be described by a coefficient of restitution.

This paper is organized as follows. Collisions between particles characterized by $St_o \gg 1$, where the Stokes number, $St_o \equiv 4mU_o/3\pi\mu_o a^2$, denotes the relative importance of particle inertia and viscous effects, are treated in § 2. In this limit, the particles move with constant speeds to leading order. We determine the viscous dissipation in both continuum and non-continuum compressible flows. In § 3, the collision process is studied for finite values of the particle Stokes number. Finally, the results are summarized in § 4.

2. Collision between particles with infinite Stokes numbers

In this section, we consider collisions between particles whose inertia is sufficiently large so that the change in their speed during the collision is small. When the particles come into contact they are assumed to undergo perfectly elastic solid-body collisions.

Figure 1 is a sketch of the geometry of the two-sphere system. Here $h'(t')$ is the minimum distance of separation at any instant of time t'. The two spheres have radii equal to a. In the lubrication limit the spherical surfaces may be approximated as paraboloids. This enables us to write the following approximate expression for the gap thickness $H'(r', t')$:

$$H'(r', t') = h'(t') + r'^2/a + O(r'^4/a^2). \tag{2.1}$$

The analysis in this section may also be used to treat spheres of different radii a_1 and a_2, if a is interpreted as twice the reduced radius, $2a_1a_2/(a_1 + a_2)$. The relative velocity of the spheres is $2U'$.

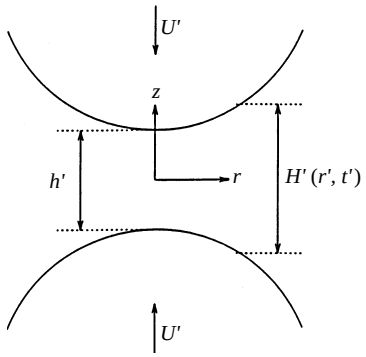

FIGURE 1. Sketch of the geometry involved in the collision between two spheres. The surfaces can be modelled as paraboloids and the gap width H' at radial position r' and time t' is given by $H'(r', t') = h'(t') + r'^2/a$, where a is the radius of the spheres.

2.1. *Compressible continuum flow*

The case of continuum flow could be studied as the limiting form for $\alpha_o \gg 1$ of the general non-continuum flow analysis that we will present in the following subsection. However, it is easier to understand conceptually and so we address it first.

Let l be the characteristic gap thickness at which the flow deviates significantly from continuum incompressible flow. For a compressible continuum flow, $l = h_c$, while it is a function of α_o for a non-continuum flow. We scale all lengths in the z-direction by l, all distances in the radial direction, r, by $(al)^{1/2}$ and the axial velocity, u'_z, by $2U_o$. The time t' is scaled by $l/(2U_o)$, the radial velocity, u'_r by $2U_o(a/l)^{1/2}$ and the pressure p' by p_o. We will henceforth represent dimensionless quantities by unprimed variables and will not write down explicitly the time dependence of variables. Using the above scalings, the dimensionless gap thickness can be written as

$$H = h + r^2. \tag{2.2}$$

As in the standard lubrication analysis, the local flow in the gap between the particles can be approximated as pressure-driven flow through a channel of width $H'(r', t')$. The inertia of the gas can be neglected provided that

$$\frac{\rho_o U_o h'_o}{\mu_o} \ll 1,$$

where ρ_o is the bulk density of the fluid. Scaling the z-momentum equation shows that the variation of the pressure and density across the gap is small compared with the radial variation. Therefore, an equation for the density can be obtained by integrating the mass conservation equation,

$$\frac{\partial \rho'}{\partial t'} + \nabla' \cdot (\rho' \boldsymbol{u}') = 0, \tag{2.3}$$

across the gap to yield

$$H\frac{\partial \rho}{\partial t} + 2\rho U + \frac{1}{r}\frac{\partial}{\partial r}(r\rho j) = 0. \tag{2.4}$$

In the above equation, U is half of the z-component of the dimensionless relative velocity of the spheres at time t. U is negative when the spheres approach one another and is positive when they rebound. Variable j represents the scaled pressure-driven

radial volumetric flux of fluid in the gap. It is a function of both r and t and is determined by solving the Stokes equations.

The partial differential equation for the pressure in the gap, (2.4), has to be solved with the following initial and boundary conditions:

$$h(t=0) = h_o, \tag{2.5}$$

$$\lim_{r\to\infty} p = 1, \tag{2.6}$$

and

$$\left(\frac{\partial p}{\partial r}\right)_{r=0} = 0. \tag{2.7}$$

The last equation follows from the symmetry of the problem.

Since the speeds of the colliding particles are constant during approach and rebound, $U = \mp\frac{1}{2}$, where the $-$ sign is used for the approach and the $+$ sign for the rebound. Similarly, during the approach, h is related to t by

$$h = h_o - t.$$

Once the relevant expression for the flux is known, equations (2.4)–(2.7) can be solved for the unknown variable p. The starting point in deriving an expression for the continuum flux is the equation of motion,

$$\rho' \frac{\mathscr{D}\boldsymbol{u}'}{\mathscr{D}t'} = \nabla' p' + \mu_o \nabla' \cdot (\nabla' \boldsymbol{u}') + \tfrac{1}{3}\mu_o \nabla' (\nabla' \cdot \boldsymbol{u}'). \tag{2.8}$$

The non-dimensional form of the r- and z-components of the momentum equation are

$$\frac{\partial p}{\partial r} = \frac{\partial^2 u_r}{\partial z^2} + O(Re_l h_o^{-3/2}) + O(la^{-1}h_o^{-3/2}),$$

and

$$\frac{\partial p}{\partial z} = O(la^{-1}h_o^{-2}) + O(Re_l la^{-1}h_o^{-1}).$$

Here, $Re_l = (U_o \rho_o l/\mu_o)$ is the Reynolds number based on the characteristic length scale l. The effects of compressibility on the momentum equations can be neglected so long as $Re_l \ll 1$, $h_o \gg 1$ and $l \ll a$. The terms characterizing the fluid inertia are small and can be neglected if $(Re_l h_o'/a) \ll 1$. In addition, the gas may be approximated as isothermal since the Péclet number is small for small Reynolds number (the Prandtl number for a gas being an $O(1)$ quantity). Scaling all variables appropriately and integrating the momentum equations gives us the following expression for the radial component of the gas velocity in the gap:

$$u_r = \frac{H^2}{8}\frac{\mathrm{d}p}{\mathrm{d}r}\left[\left(\frac{2z}{H}\right)^2 - 1\right].$$

Integrating the radial velocity across the gap thickness gives the flux as a function of r.

$$j = -\frac{H^3}{12}\frac{\mathrm{d}p}{\mathrm{d}r}. \tag{2.9}$$

It should be noted that this result is valid for both compressible and incompressible continuum flow. Thus the equation governing the pressure profile in the gap is obtained by substituting (2.9) in (2.4).

The numerical scheme used to integrate the partial differential equation for the pressure consisted of a predictor-corrector method in time and finite differences in radial position. A transformed radial variable, $r^* = r/(r+1)$, was used so that the spatial domain was transformed from $(0, \infty)$ to $(0, 1)$. The boundary condition for the pressure at $r = \infty$ corresponding to $r^* = 1$ could then be implemented easily. In addition, convergence of the numerical solution was tested by varying the size of both the time and space grids. It was found that converged results for the force on the spheres were obtained when 200 or more grid points (for r^*) were used. In all cases, the numerical calculations were started with large enough values of h_o that the initial flow was nearly incompressible. In obtaining the results in this section, it was assumed that contact between particles occurred when the gap thickness was reduced to $O(10^{-3})$. This leads to a small error in the total viscous dissipation during the approach.

A regular perturbation analysis in the limit $h \gg 1$ can be used to find the first effects of compressibility. The expression for the pressure has the form

$$p = 1 + p_1 + p_2 + p_3 + \ldots \tag{2.10}$$

where $p_i(0, t)$ is order h^{-2i}. Here, $1 + p_1$ is the pressure for incompressible flow. The terms in the expansion are given by

$$p_1 = \frac{3}{2H^2}, \quad p_2 = -\frac{9}{8H^4} - \frac{3}{2hH^3},$$

and

$$p_3 = \frac{27}{16H^6} + \frac{117}{40hH^5} + \frac{63}{32h^2H^4} + \frac{33}{8h^3H^3}.$$

Numerical calculations were conducted with $h_o = 20$. The approximate pressure distribution given by (2.10) was used as the initial condition. The pressure profile for the gas in the gap during approach at $h = 1$ is shown in figure 2. As expected, compressibility reduces the pressure compared with that which would arise in an incompressible fluid. For an incompressible lubrication flow, the pressure in the gap has to be sufficient to drive enough fluid out of the gap to compensate for the volume swept out by the approaching particles. However, when the gap becomes sufficiently thin, the gas can compress with a smaller increase in pressure than that required to drive an incompressible fluid out of the gap.

An asymptotic analysis can be performed in the limit $h \ll 1$. For extremely small gap thicknesses, the radial flux term is negligible because the gas tends to compress rather than flow out. By equating the first two terms in (2.4), we can obtain the following expression for the pressure:

$$p = A(r)/H.$$

Here, A is a function of radial position that is controlled by the flow occurring when $h \sim O(1)$. Figure 3 is a plot of Hp as a function of the scaled radial distance, r, for various values of h. As $h \to 0$ the curves are seen to approach a limiting curve $A(r)$ in agreement with the asymptotic expression for p.

By symmetry, the force acting on each sphere, F', is in the z-direction. Its value can be obtained by an integration of the pressure over the surface of the sphere. It is interesting to see how this compares with the force for the incompressible case. We define f as the ratio of the actual force to the force the particle would have experienced at the same separation in an incompressible fluid, namely $f = F'/F'_{in}$,

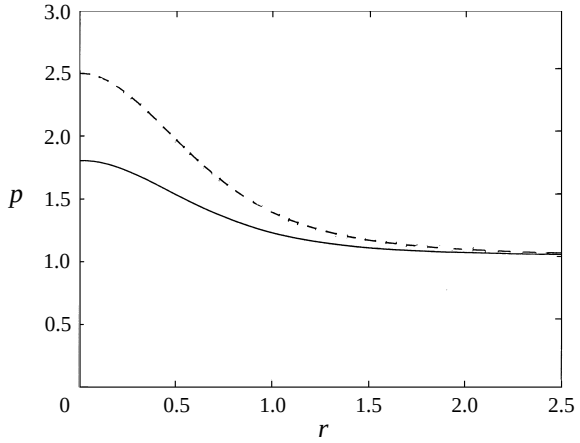

FIGURE 2. The radial pressure profiles in the gap during the approach when $h = 1$. The solid line is the result for continuum compressible flow, while the dashed line shows the profile for a continuum incompressible flow.

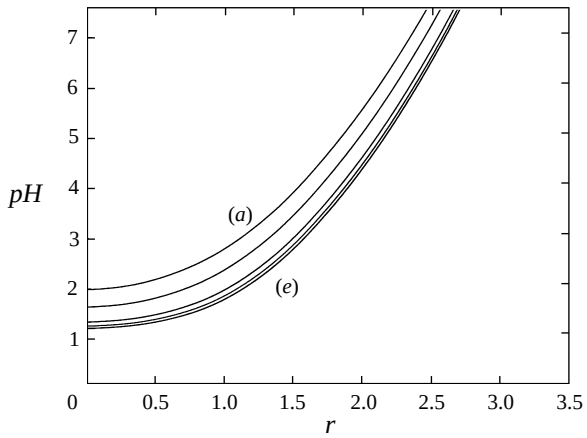

FIGURE 3. For a compressible continuum flow, $H(r, h)p(r)$ asymptotes to a limiting curve as $h \to 0$. All the profiles correspond to the approach. The curve marked (a) corresponds to $h = 1.25$ and the others to $h = 1, 0.25, 10^{-2}$ and 10^{-4}. For values of $h = 10^{-4}$ and smaller, the profiles essentially collapse to the curve marked (e).

where $F'_{in} = 6\pi\mu_o a^2 U_o/h'$. The approximate expression for f in the asymptotic limit $h \gg 1$ may be obtained using (2.10) and it has the form

$$f = 1 - \frac{3}{4}\left(\frac{1}{h^2}\right) + \frac{101}{40}\left(\frac{1}{h^4}\right) + O\left(\frac{1}{h^6}\right). \tag{2.11}$$

In the limit $h \ll 1$, the centreline pressure diverges like h^{-1}, and so we expect the force to diverge as $\log h$. Figure 4 is a plot of the non-dimensional force, F, as a function of h during the approach. The asymptotes corresponding to $h \gg 1$ and $h \ll 1$ are also shown. The asymptote for $h \gg 1$ is seen to match the actual curve very well for $h > 5$. In the limit $h \to 0$, the force has a logarithmic dependence on the gap thickness:

$$\lim_{h\to 0} F \sim \quad 0.38 - 0.8 \ln h, \tag{2.12}$$

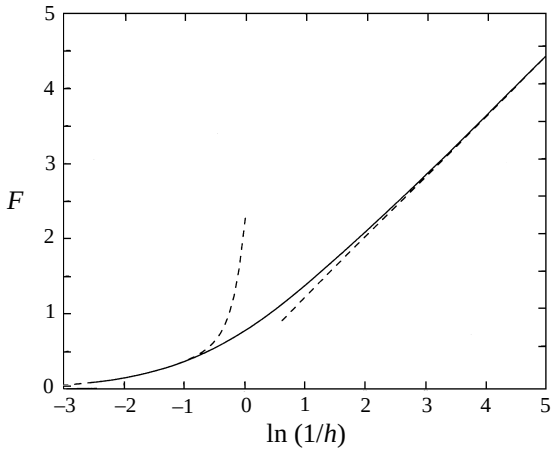

FIGURE 4. A plot of F as a function of h, during the approach for a compressible continuum flow. The solid line corresponds to the calculated values. The two dashed lines are the asymptotic expressions for $h \gg 1$ and $h \ll 1$. As $h \to 0$, F diverges logarithmically. This implies that the total energy dissipated in the approach is finite.

where the constants in (2.12) were chosen to give a best fit to the numerical results at small h.

Figure 5 is a plot of f, the ratio of the force to the force corresponding to incompressible flow, as a function of h during the approach and rebound of two particles. The dotted line is the asymptote given by (2.11) corresponding to $h \gg 1$. The solid line corresponds to the approach while the dash-dot line is the rebound. The divergence of the force caused by a compressible fluid is weaker than that for an incompressible fluid, so $f \to 0$ as $h \to 0$. When the sphere first begins to rebound, the fluid exerts a force in the same direction as the particle's motion. This launching force comes from the expansion of the compressed gas in the gap as the energy that was stored in the gas during the approach is transferred to the particle. At $h \approx 0.5$ the force reverses direction and resists the particle motion.

It is interesting to observe that f becomes greater than 1 at $h \approx 1.8$ during the rebound process, indicating that the resistance to rebound is larger than the corresponding value for a collision in an incompressible fluid. During the initial portion of the rebound, the gas in the gap expands more easily than new gas can be drawn into the gap. As the gap widens and viscous flow becomes feasible, an extra flux is necessary to make up for the small inward flux at early time. A larger pressure drop is required to drive this flux than that in an incompressible flow. As the gap thickness increases further, the compressibility of the gas becomes unimportant and so f approaches 1 as h becomes much greater than 1.

Figure 6 shows the pressure profiles for three values of h during the rebound. At $h = 0.18$, the pressure is larger than 1 due to the compression of the gas that occurred during the approach. As the particles recede and the gas expands, the pressure eventually decreases below the atmospheric pressure so that gas is once again drawn into the gap. It is interesting to note that there are three extrema of the pressure at $h = 0.843$. Near the centreline, the pressure is still above 1, because of the compression that occurred during the approach. However, the gas at $r \approx 0.6$ has already expanded to a subatmospheric pressure. As a result, the gas flux is outward for $r < 0.6$ and inward for $r > 0.6$.

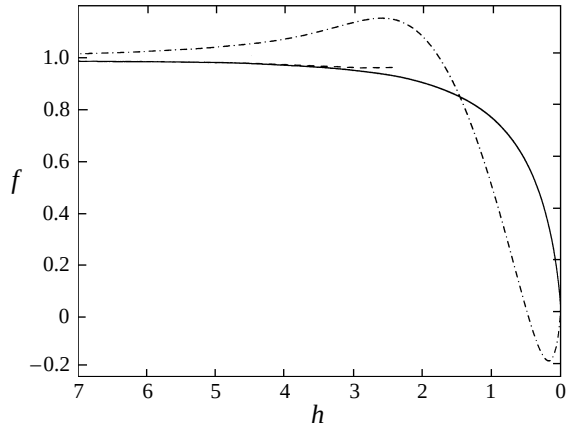

FIGURE 5. The variation in f during the course of the collision for a compressible continuum flow. The solid curve corresponds to the approach and the dash-dot line to the rebound. The dashed line is the asymptotic expression for f when $h \gg 1$. As $h \to 0$, $f \to 0$ showing that the divergence of the force is weaker than the h^{-1} divergence for an incompressible continuum flow.

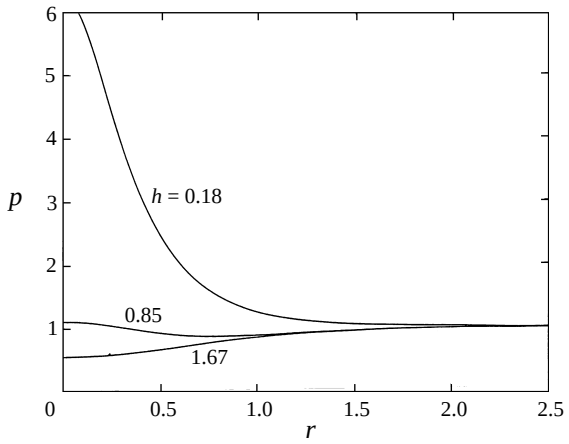

FIGURE 6. The radial pressure profiles in the gap during the rebound for a compressible, continuum flow. The profiles shown are for $h = 0.18, 0.85$ and 1.67. When $h \approx 0.85$, the pressure in the gap is less than p_o, the bulk pressure, and the profile exhibits three extrema.

The force acting on particles colliding in an incompressible fluid diverges like $1/h$, so that the work, defined as the integral of F over all separations h, diverges. However, the compressibility of the gas leads to a weaker growth of the force at small separations, cf. (2.12), and a convergent result for the work. In general, for arbitrary α_o, the expression for the energy dissipated during the approach can be written as follows:

$$W_a' = 3\pi\mu_o a^2 U_o \, [\ln(h_o'/h_c) + K_a]. \tag{2.13}$$

The subscript a denotes the fact that this dissipation occurs during the approach. The first term is the dissipation that would occur if the force were given by the incompressible, continuum flow result for all $h' > h_c$ and by zero otherwise. The

constant K_a, representing the deviation from this crude estimate, is given by

$$K_a = \frac{1}{3\pi\mu_o a^2 U_o'} \int \mathrm{d}h' [\, F' - F_{in}' H(\, h' - h_c)\,], \tag{2.14}$$

where the Heaviside step function, $H(h' - h_c)$, is zero if $h' < h_c$ and 1 otherwise. From the above formulation we expect K_a to be an $O(1)$ number for compressible continuum flow. Our numerical results indicate that K_a is approximately 1.17 for a continuum compressible flow. For the general non-continuum flows treated in the next subsection, K_a will be a function of α_o and will diverge as $\alpha_o \to 0$.

The work done against the fluid during rebound can be written in a form similar to (2.13) so that the total energy dissipated in the collision may be expressed as

$$W_T' = 3\pi\mu_o a^2 U_o\, (2\ln(h_o'/h_c) + K), \tag{2.15}$$

where

$$K = K_a + K_r.$$

Here K_r is a constant similar to K_a appearing in the analogous equation for the dissipation during rebound. In calculating K_r we have assumed that the collision process ends when the particles have rebounded back to their initial separations. Again, for a general non-continuum flow K and K_r will be functions of α_o. The value of K_r for compressible continuum flow is negative ($= -1.34$) showing that some of the work done during the approach is stored in the compressed gas and is released during rebound. An estimate of the magnitude of the energy stored may be obtained as the difference between K_a and K_r.

2.2. *Compressible non-continuum flow*

When $\alpha_o \sim O(1)$, the effects of the compressibility and the non-continuum nature of the gas flow are of equal importance. In this case, we need to redefine the characteristic gap width, l, at which the standard lubrication analysis needs to be modified. Clearly, as $\alpha_o \to \infty$, $l \to h_c$ and as $\alpha_o \to 0$, $l \to \lambda_o$. We choose to define l as

$$l = h_c \frac{1 + \alpha_o}{\alpha_o}. \tag{2.16}$$

Since the gas flow is discrete in nature, it is no longer possible to use the continuum equations of momentum conservation to derive an expression for the flux. However, Sundararajakumar & Koch (1996) showed that under conditions of small Mach number, the momentum equation obtained by averaging the Boltzmann equation for the gas flow in the gas is unaffected (to leading order) by the compressible nature of the gas. Thus, the compressible continuum lubrication analysis derived above can be extended to finite values of α_o if the continuum Poiseuille flux relationship is replaced by a solution of the linearized Boltzmann equation for the pressure-driven incompressible fluid flow between two plates separated by a distance H. As in the continuum case, compressibility effects have to be taken into account in the mass conservation equation. Thus the governing equation for the pressure for a general compressible non-continuum flow is (2.4) with the value of j modified to account for the discrete nature of the gas flow.

The pressure-driven mass flux may be written in the form

$$j = -\frac{2H^2(1 + \alpha_o)}{3\pi\rho\alpha_o^2}\, Q(\delta)\, \frac{\partial p}{\partial r}, \tag{2.17}$$

where $\delta = (H'/\lambda)$, and λ is the local mean free path based on the instantaneous local pressure. The flux function $Q(\delta)$ is obtained from different expressions depending on the numerical value of δ. For $\delta > 10$, the effects of non-continuum flow may be approximated in terms of a Maxwell slip boundary condition on the particle surfaces and $Q(\delta)$ in this range is given by (Hocking 1973)

$$Q(\delta) = \tfrac{3}{4}\pi(1 + \tfrac{1}{6}\delta).$$

When $0.1 < \delta < 10.0$ we use the results of a numerical solution of the Bhatnagar–Gross–Krook (BGK) approximation to the linearized Boltzmann equation presented by Cercignani & Daneri (1963). In the range $\delta < 0.1$, the expression obtained by Sundararajakumar & Koch (1996) is used:

$$Q(\delta) = -\ln\delta + 0.4531.$$

The boundary conditions for the pressure and the initial condition for h are the same as for continuum compressible flow, i.e. (2.5)–(2.7).

For the case where the compressibility of the gas is negligible, i.e. $\alpha_o \to 0$, Hocking (1973) derived the following expression for the pressure in the gap including the first non-continuum effects:

$$p = 1 - \tfrac{1}{12}\alpha_o^2\,(\,\ln(1 + 6/\delta) - 6/\delta\,). \tag{2.18}$$

The pressure and force for an incompressible non-continuum flow, valid for all δ was derived by Sundararajakumar & Koch (1996).

All of the numerical calculations were started from values of h_o large enough so that the initial flow corresponded to nearly incompressible continuum flow. The pressure distribution in (2.18) was used as the initial condition for p when solving the partial differential equation. The value of δ at $t = 0$ was evaluated using the atmospheric pressure, p_o, because the pressure change in the gap is small compared to p_o at large values of h. However as h becomes close to 1, the pressure change is more pronounced and the dependence of the mean-free path on p cannot be neglected. We used the pressure profile obtained in the previous time step to determine the mean-free paths in the predictor step, and then used the results for the pressure obtained in the predictor step to evaluate the mean free paths in the corrector step. In this way, δ and $Q(\delta)$ can be evaluated at every radial position.

The results for f, the ratio of the force to the incompressible continuum result, are plotted in figures 7–10 for different values of the parameter α_o. Figures 7 and 8 show the dynamics of approach while figures 9 and 10 show the results for the rebound. It is evident from the profiles for the approach that the force on the spheres becomes smaller than the continuum force as h decreases and as the non-continuum/compressible nature of the gas becomes more important. The divergence of the actual force is weaker than that of the incompressible continuum force, as indicated by the fact that $f \to 0$ as $h \to 0$. The force also decreases with decreasing α_o due to the increasing importance of non-continuum effects. Sundararajakumar & Koch (1996) showed that the divergence of the force for an incompressible non-continuum flow is $\ln\ln(1/h)$ as $h \to 0$, which is weaker than the divergence predicted for a continuum compressible flow. This is in agreement with our numerical results.

The force tending to push the particles apart during the initial stages of the rebound diminishes as α_o decreases, indicating that the fraction of the initial kinetic energy stored due to compressibility decreases. The minimum in the profiles during the rebound, as shown in figures 9 and 10, is also seen to shift upwards and towards $h = 0$. These trends arise because, for small α_o, the force diminishes as a result of the

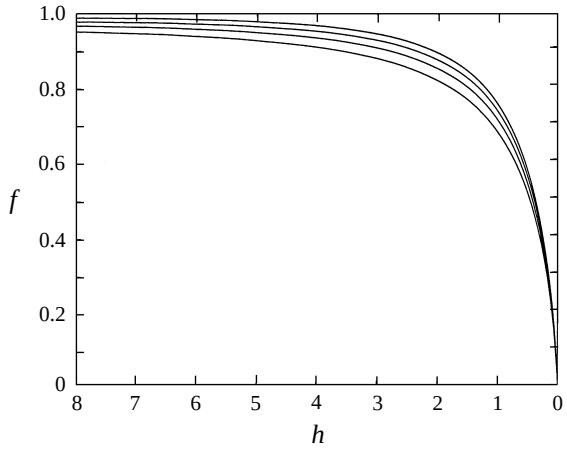

FIGURE 7. Plots of the scaled force, $f(h, \alpha_o) = F'/F'_{in}$ during the approach, for different values of α_o. The curves shown correspond to (from the uppermost curve) $\alpha_o = \infty, 25, 10$ and 5. As $\alpha_o \to 0$, the force on the sphere steadily decreases.

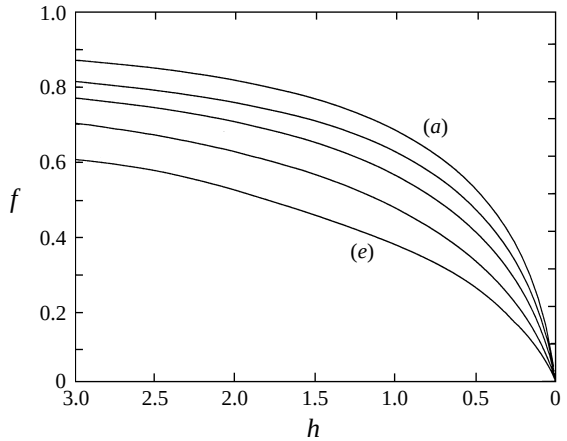

FIGURE 8. Plots of $f(h, \alpha_o)$ during the approach, for (from the uppermost curve marked (a)) $\alpha_o = 5, 2, 1$ and 0.3. The lowest curve (e) is for $\alpha_o = 0$, which corresponds to incompressible non-continuum flow.

finite mean-free path before compressibility becomes important. In the limit $\alpha_o \to 0$, the flow is quasi-steady and the force during rebound is just the mirror image of that during approach. The results for α_o greater than 50 are within 5% of the continuum compressible result. For values of α_o smaller than 0.3 (figures 8 and 10) the curves start to collapse and approach the non-continuum incompressible limit. For $\alpha_o < 0.09$, the results were within 5% of that for $\alpha_o = 0$.

It is interesting to consider the variation of the energy dissipated during the approach and rebound with varying α_o (figures 11 and 12). Consider the total work done, W'_T in the form written earlier in (2.15). The asymptotic behaviour of $K(\alpha_o)$ in the two limits has been determined in the previous subsection and in Sundararajakumar & Koch (1996), and is given by

$$\lim_{\alpha_o \to \infty} K(\alpha_o) \sim -0.18,$$

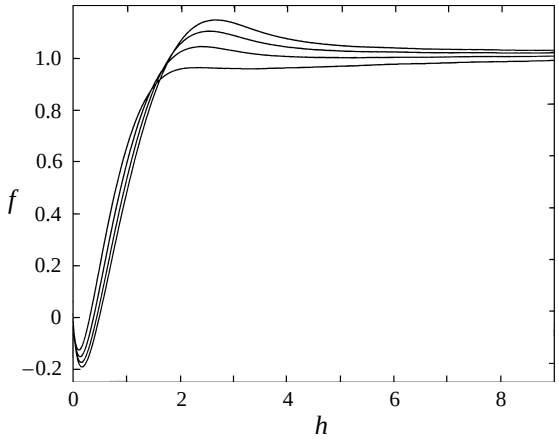

FIGURE 9. Plots of $f(h, \alpha_o)$ during the rebound, for $\alpha_o = \infty, 25, 10$ and 5. As $h \to \infty$, all the curves approach 1. It is clear that the force tending to push the particles apart during the initial stages of the rebound diminishes with decreasing α_o.

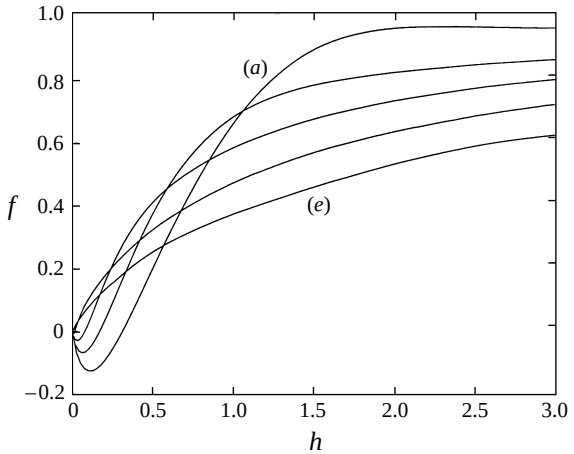

FIGURE 10. Plots showing $f(h, \alpha_o)$ during the rebound process. The curve marked (a) corresponds to $\alpha_o = 5$, and (e) corresponds to $\alpha_o = 0$. The intermediate curves are results for $\alpha_o = 2, 1$ and 0.3. The curve for $\alpha_o = 0$ is same as that for the approach plotted in figure 8.

and

$$\lim_{\alpha_o \to 0} K(\alpha_o) \sim -2.56 + 2 \ln \alpha_o.$$

The $\ln \alpha_o$ dependence of K_a for small α_o reflects the fact that the dissipation is controlled by the mean-free path of the gas rather than by h_c in this limit. One can also consider only the energy loss during the approach. This loss not only includes viscous dissipation but also the energy stored due to the compressibility of the gas. The asymptotic values of $K_a(\alpha_o)$ are as follows:

$$\lim_{\alpha_o \to \infty} K_a(\alpha_o) \sim 1.17,$$

and

$$\lim_{\alpha_o \to 0} K_a(\alpha_o) \sim -1.28 + \ln \alpha_o.$$

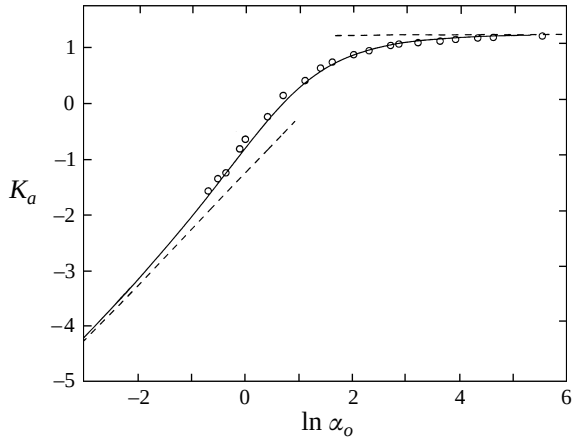

FIGURE 11. Plot of $K_a(\alpha_o)$ as a function of α_o. Also shown as dashed lines are the two asymptotes for non-continuum incompressible ($\alpha_o \ll 1$) and continuum compressible ($\alpha_o \gg 1$) flow. The circles are the numerically calculated values and the solid curve corresponds to (2.19).

For intermediate values of α_o, the following approximate expression fits the numerical data quite well:

$$K_a(\alpha_o) = \frac{1.708\ (-1.28 + \ln \alpha_o\ ) - 1.2424\alpha_o + 0.8090\alpha_o^2}{1.708 + 0.71676\alpha_o + 0.6942\alpha_o^2}. \tag{2.19}$$

Figure 11 is a plot of K_a as given by (2.19). The dashed lines indicate the asymptotic behaviour for $\alpha_o \to 0$ and $\alpha_o \to \infty$. K_a is seen to increase monotonically with increasing α_o.

Figure 12 is a plot of K_r as a function of α_o. The solid curve is a spline fit to the numerical results while the dotted lines are the asymptotic results. Unlike K_a, K_r is seen to exhibit a maximum when $\alpha_o \sim O(1)$. This may be explained as the result of two competing effects. For large values of α_o, the gas expands significantly during the early stages of the rebound, accelerating the relative motion of the particles and thus reducing the net value of the work done by the spheres on the gas. As α_o decreases, the energy imparted to the sphere by this compressed gas also decreases leading to an increase in the net work done on the gas. However, at the same time the increasing non-continuum nature of the flow results in a reduced drag force. Thus as the value of α_o is reduced starting from $\alpha_o \gg 1$ the net work increases slightly and then decreases as $\alpha_o \to 0$.

K_a includes the energy spent in compressing the gas. Hence one could define a new variable, $K_d = K_a - K_r$, which is the energy stored in the compressed gas during the approach and released during rebound. Like K_a, K_d is a monotonic function of α_o. An approximate expression for K_d obtained by a curve fit is

$$K_d(\alpha_o) = \frac{\alpha_o + 0.027\alpha_o^2}{1.10 + 0.39\alpha_o + 0.012\alpha_o^2}. \tag{2.20}$$

The differences between this expression and the numerically calculated values are less than 5%.

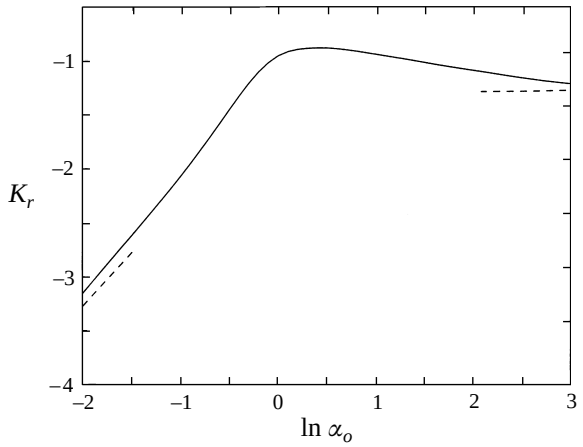

FIGURE 12. Plot of $K_r(\alpha_o)$, as a function of α_o. The solid curve is a spline fit to the actual values, while the dotted lines are the asymptotes for small and large values of α_o. The curve exhibits a maximum when $h \sim O(1)$.

3. Dynamics of collisions for finite Stokes number

In this section, we consider the dynamics of collisions between particles with finite inertia. The incompressible lubrication flow at low Reynolds number is quasi-steady and so one can decouple the dynamics of the particle from the determination of the force and express the force at time t as a function of the gap thickness and relative velocity at time t. This situation applies even to non-continuum flows (Sundararajakumar & Koch 1996). However, the compressibility of the gas makes the flow unsteady and one must solve the dynamics of the particle acceleration and the fluid compression as a coupled problem.

The Stokes number for particles with radii of 10–100 μm whose relative velocity is comparable with their terminal velocities will be $O(100)$ or greater. For such situations, the large-Stokes-number asymptote derived in the previous Section will suffice. However, the relative velocity may be substantially less than the terminal velocity. For example, a typical relative velocity in particulate fluidization is about 1% of the terminal velocity. Also, if one is interested in aggregation driven by differential sedimentation, it is the difference in the terminal velocities of two particles that is relevant.

Whereas the results of the previous Section could be applied to a pair of particles with different sizes and velocities, we restrict our attention here to particles with identical radii a and equal and opposite initial velocities $\mp U_o$. The generalization to different particle radii and initial speeds is straightforward but would require a separate calculation because of the coupling between the dynamics of the particles and that of the gas flow.

The governing equations and the initial and boundary conditions are identical to those described in the preceding section. However, we must now also solve

$$St_o \frac{\mathrm{d}U}{\mathrm{d}t} = F, \tag{3.1}$$

$$\frac{\mathrm{d}h}{\mathrm{d}t} = 2U, \tag{3.2}$$

for the relative velocity of the particles and the gap thickness as a function of time.

Here F is the instantaneous drag force acting on a single sphere made dimensionless by $(3\pi\mu_o a^2 U_o/l)$, and St_o is the Stokes number based on the initial speed. In general, the flow is not quasi-steady, i.e. $F(t)$ is not proportional to $U(t)$.

3.1. *Incompressible continuum flow*

We begin by reviewing the dynamics of particles subject to the standard incompressible continuum lubrication force. This provides simple analytical results that may be used for comparison with the solutions including non-continuum effects and compressibility.

Equations (3.1) and (3.2) may be combined with the expression for the continuum, incompressible lubrication force to obtain an equation for $\mathrm{d}U/\mathrm{d}h$. Integrating this equation yields

$$U = \frac{1}{2} - \frac{1}{St_o}\ln\frac{h_o}{h}. \tag{3.3}$$

In addition, F is related to U through

$$F = \frac{U}{2h}. \tag{3.4}$$

Thus F goes to zero when U goes to zero, ruling out the possibility of a rebound. Equation (3.3) indicates that the relative velocity of the two particles will be arrested at a separation

$$h_{min} = h_o \mathrm{e}^{-St_o/2}, \tag{3.5}$$

and the particles never come into contact.

3.2. *Incompressible non-continuum flow*

In this case, the finite mean-free path of the gas allows the particles to achieve solid-body contact provided that (Sundararajakumar & Koch 1996)

$$St_o > 2\,(\ln(h_o'/\lambda_o) - 1.28).$$

The fraction of the initial energy dissipated before contact, $1 - e_{va}^2$, can be obtained using

$$1 - e_{va}^2 = \frac{4}{St_o}(\ln(h_o'/\lambda_o) - 1.28)\left(1 - \frac{1}{St_o}(\ln(h_o'/\lambda_o) - 1.28)\right). \tag{3.6}$$

If the particles undergo a perfectly elastic collision upon contact and

$$St_o > 4\,(\ln(h_o'/\lambda_o) - 1.28),$$

then the particles will return to their initial separation, h_o', after the collision. The total energy dissipated during the approach and rebound is

$$1 - e_v^2 = \frac{8}{St_o}(\ln(h_o'/\lambda_o) - 1.28)\left(1 - \frac{2}{St_o}(\ln(h_o'/\lambda_o) - 1.28)\right). \tag{3.7}$$

In (3.6) and (3.7), e_{va} and e_v may be interpreted as effective coefficients of restitution for the approach and for the overall collision when only losses due to viscous dissipation are considered.

3.3. *Compressible continuum flow*

Having reviewed the known results for incompressible lubrication flows, we now consider the coupled dynamics that arise when two particles with finite inertia collide

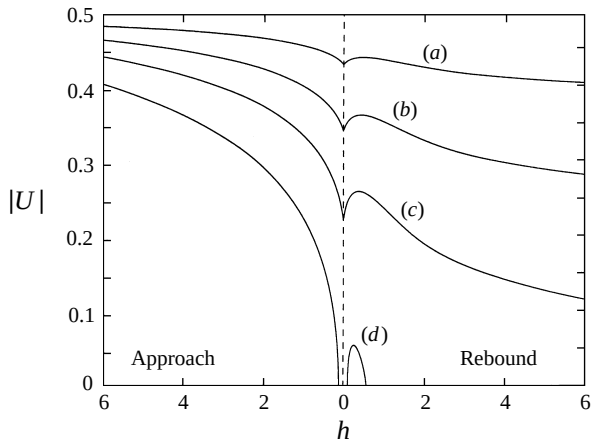

FIGURE 13. Profiles of $|U|$ for a compressible continuum flow as a function of the minimum gap width, h, for different values of the Stokes number, St_o. The curves labelled $(a), (b), (c)$ and (d) correspond to $St_o = 55.32, 25.32, 15.32$ and 9.32 respectively. For $St_o = 9.32$, the spheres are seen to rebound without actually coming into contact.

in a compressible gas. We begin our study with the continuum limit and include the finite mean-free path of the gas in the following subsection. We solve equations (2.4)–(2.7) with the continuum expression for the flux, (2.9), and the equations relating h and U to F given by (3.1) and (3.2). All the computations shown are for an initial separation of $h_o = 100/7$.

Figure 13 shows the variation in the velocity of sphere 1 as a function of h for various values of St_o. For the case of infinite St_o, $|U| = 1/2$ for all h. For large values of the Stokes number ($St_o \approx 55.3$ and 25.3), the change in the particle speed is small and hence the particles collide with a finite velocity and rebound back to their initial separations. As St_o is decreased, the velocity when the particles rebound back to their initial separation reduces significantly until for $St_o = St_2$ this velocity becomes zero. For $h_o = 100/7$, $St_2 \approx 14.9$. On reducing the Stokes number further, the final separation between the spheres reduces until the spheres are barely able to collide. This occurs for $St_o = St_1$ where $St_1 \approx 10.3$ for $h_o = 100/7$. For lower values of the Stokes number ($< St_1$) the spheres come to a stop before they can collide with one another as all the kinetic energy is lost by viscous dissipation.

Figure 13 also illustrates an interesting phenomenon related to the energy stored in the compressed gas. For $St_o > St_1$ the energy stored in the compressed gas is released during rebound and hence the velocity during the rebound increases and reaches a maximum before decreasing due to viscous drag. As the Stokes number decreases, the difference between this maximum velocity and the velocity immediately after impact increases and reaches a maximum after which it decreases to zero. The energy stored in the compressible gas also provides the possibility that the particles can rebound without actually making solid-body contact. This is seen in the figure for $St_o = 9.32$. The particle actually underwent several damped oscillations; however only the first is evident on the scale of the figure. As the Stokes number decreases further, less energy is stored in the gas and the amplitude of the rebound decreases.

Barnocky & Davis (1989) have observed particle rebounds without direct physical contact due to the compressibility of a liquid at sufficiently high Stokes numbers. Kytömaa & Schmid (1992) argued that such a rebound could not occur if one

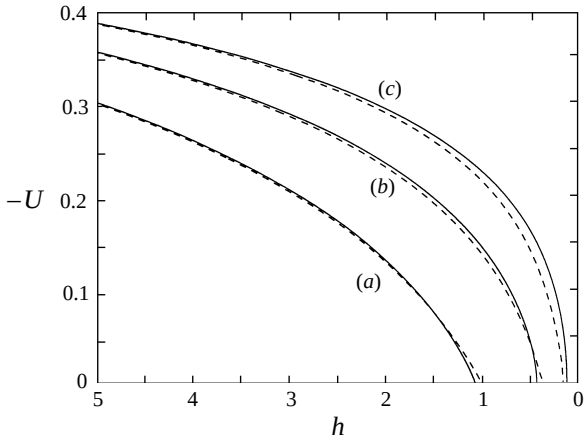

FIGURE 14. Plot of the velocity as a function of the minimum gap thickness h, during the approach, for $St_o = 9.32, 7.32$ and 5.32 (curves marked c, b and a), when $\alpha_o = \infty$. The corresponding results for incompressible continuum flow are shown as dashed curves. The value of h_o is $100/7$.

considered only linear compressibility effects and corroborated this argument with an analysis of (2.4) in the limit of large h. Although the relationship between the pressure and density in the ideal gas studied here is linear, we have retained higher-order terms in (2.4) and thereby obtained particle rebound without solid-body contact over a narrow range of Stokes numbers.

For a fixed value of h_o, the flow becomes more nearly incompressible as the Stokes number, St_o, decreases. This is illustrated in figure 14 which is a plot of the dimensionless velocity during the approach, as a function of h for small St_o, The dotted lines are the velocities predicted based on incompressible flow, namely (3.3). The velocity for the compressible fluid is quite close to the incompressible result for $St_o < 5.32$. For $St_o = 9.32$ the velocity deviates noticeably from the incompressible result and the minimum distance of approach is less than that predicted by the incompressible result. As noted before, in this case the spheres were seen to rebound even though actual contact between the particles did not occur. Another feature observed in this figure is that for very small St_o, the minimum distance of approach is slightly greater than that predicted by the incompressible theory.

We also consider collisions in which there is a solid-body energy loss. We assume that any surface deformation that may occur does not have a substantial influence on the viscous dissipation. The energy loss due to the solid-body collision is modelled in terms of a coefficient of restitution, e_s. The only change required in our computational algorithm is that the velocity immediately after impact is now $-e_s$ times the velocity just before collision. We performed numerical calculations for $h_o = 14.28$, $St_o = 20$, and a wide range of e_s. The fraction of the initial kinetic energy of the two particles lost during the collision is plotted as a function of e_s in figure 15. We also present the fractional energy loss due to the viscous dissipation during the approach and rebound and the loss due to the solid-body collision. Although the viscous loss when $e_s = 1$ is nearly 53%, the total fractional energy loss goes to 1 only when e_s is less than 0.2. The total energy loss does not increase as rapidly as one would predict by linearly superimposing the viscous and solid-body energy losses. This is because the smaller rebound velocity for the particles with smaller e_s causes less viscous dissipation. In addition, the energy stored in compression of the gas during the approach can aid in

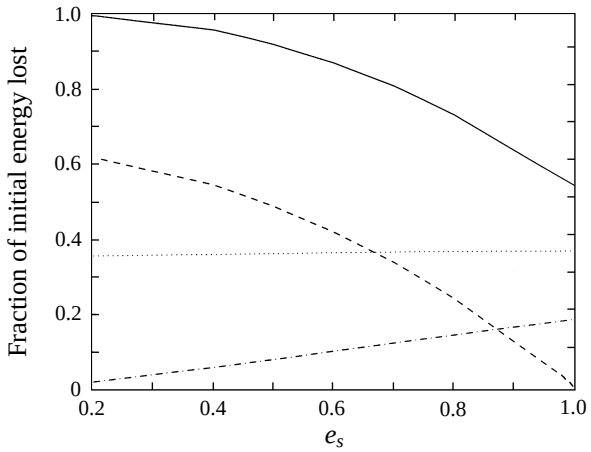

FIGURE 15. The fraction of the initial kinetic energy lost in the collision process, plotted as a function of e_s for the case $St_o = 20$, $h_o = 14.28$ and $\alpha_o = \infty$. The solid line represents the total energy lost, the dotted line is the energy lost due to viscous dissipation during the approach, the dashed line is the loss during impact and the dash-dot line is the energy lost during rebound.

the rebound of the particles and this effect becomes more important with decreasing e_s.

3.4. *Compressible non-continuum flow*

We now consider the general case in which both the compressibility and finite mean-free path of the gas are important and the particles have finite inertia. The equations governing this case are the same as those described in the previous subsection except that the expression for j is given by (2.7). As $\alpha_o \to 0$, the results reduce to the incompressible case treated in § 3.2.

Figure 16 shows the variation of the particle velocity with gap thickness for $St_o = 15.3$, $h'_o/h_c = 14.28$, and different values of α_o. We have presented the results in terms of h/h_o so that we can compare near-continuum and strongly non-continuum flows in the same plot. The dashed line corresponds to the $\alpha_o \to \infty$ asymptote, while the solid lines are for $\alpha_o = 10, 2$ and 0.8. At $\alpha_o \to \infty$, only the compressibility of the gas places a finite limit on the energy dissipation due to viscous force. As α_o decreases, however, non-continuum effects also decrease the lubrication force leading to less energy dissipation during the approach. It may be seen in figure 16 that these non-continuum effects are important primarily at small gap thicknesses. At large h', the lubrication flow approaches the continuum incompressible limit. As α_o decreases, the maximum in the velocity during the rebound decreases.

Figure 17 shows the fraction of the initial particle energy lost during the approach for collisions with $h'_o/h_c = 14.28$ and $\alpha_o = 0.8, 2, 10$, and ∞ as a function of St_o. It can be seen that the energy loss decreases with increasing α_o and so does the value of St_1 at which the particle's kinetic energy is completely dissipated at the point of contact.

Figure 18 is a plot of St_1 as a function of α_o for $h'_o/h_c = 14.28$. The circles correspond to the numerical calculations. The values of St_1 were calculated using a bisection approach with an error of less than 5%. For large values of α_o, the numerical results approach the asymptote determined in the previous subsection for continuum compressible flow, i.e. $\alpha_o = \infty$. The dot-dash curve for small α_o is the incompressible, non-continuum flow asymptote obtained using the force expressions

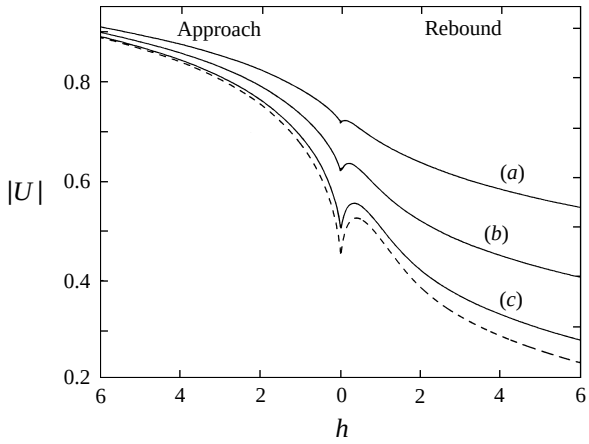

FIGURE 16. The variation in $|U|$ as a function of h and α_o during approach and rebound for the case $St_o = 15.32$ and $h_o = 14.28$. The solid curves labelled (a), (b) and (c) correspond to $\alpha_o = 0.8, 2$ and 10 respectively. The asymptote corresponding to $\alpha_o = \infty$ is shown as a dashed curve.

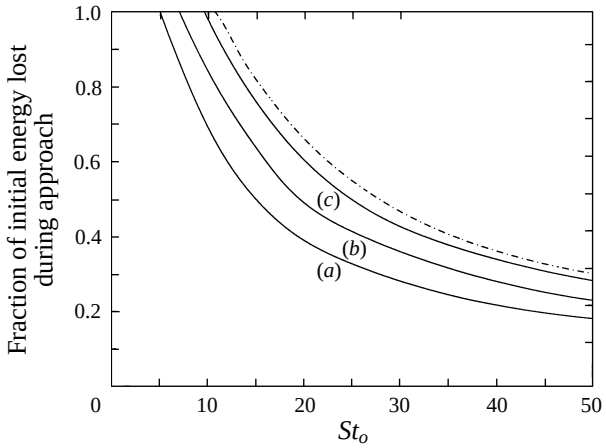

FIGURE 17. Plot showing the fractional energy lost due to viscous effects during the approach as a function of St_o for $h'_o/h_c = 14.28$, $\alpha_o = 0.8, 2$ and 10, (a), (b), (c) respectively. The dot-dash curve is the asymptote approached as $\alpha_o \to \infty$.

in Sundararajakumar & Koch (1996). It is clear that the calculated values are quite close to the incompressible asymptote for $\alpha_o < 2$. We note that St_1 goes to zero as $\alpha_o \to 0$ because we have held h'_o/h_c fixed but allowed h'_o/λ_o to approach zero.

An approximate criterion to determine St_1 for an arbitrary value of α_o and h'_o can be easily deduced based on simple physical arguments. From the results for infinite Stokes number it is clear that for $h \gg 1$, the flow is essentially incompressible. So we assume that the force for $h \geqslant 1$ may be approximated using the incompressible continuum result while the force for $h \leqslant 1$ is a constant and equal to that at $h = 1$. The critical Stokes number obtained with this simplistic force law is

$$St_1 = 2\,(\ln(h'_o/l) + 4).$$

Although the reasoning employed above is qualitatively correct, the number 4 is not accurate and is in fact a crude estimate of the $O(1)$ constant, which we denote by

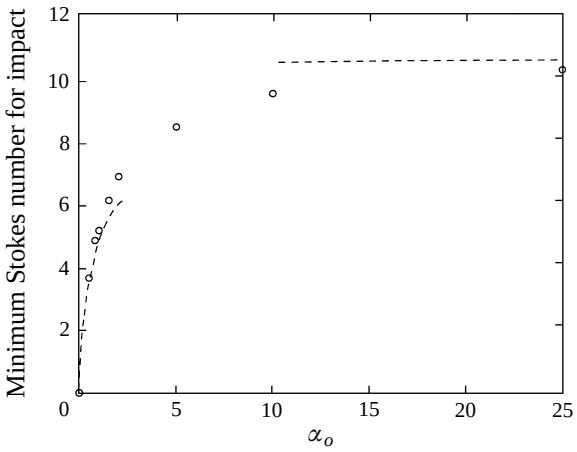

FIGURE 18. The minimum Stokes number for impact to occur, St_1, shown here as a function of α_o for $h_o = 14.28$. The dashed line at large α_o corresponds to the asymptote for compressible, non-continuum flow. The dashed curve for small α_o is obtained from the force expressions given in Sundararajakumar & Koch (1996). For small values of α_o, the actual results lie quite close to the incompressible predictions.

C, that is sensitive to the flow at small h and is virtually unaffected by the flow conditions at large h. Thus, it is independent of h_o and may be treated as a function of α_o alone. The expression for St_1, then has the form

$$St_1 = 2\,(\,\ln h_o + C(\alpha_o)\,) \tag{3.8}$$

where the function $C(\alpha_o)$ can be found by solving the diffential equations for a fixed value of h_o, which satisfies $h_o \gg 1$, so that the initial flow is incompressible and continuum. Our results show that $C(\infty) \approx 2.59$ and from (3.6) we find that $C(0) \approx -1.28$. Figure 19 is a plot of $C(\alpha_o)$ as a function of α_o. The solid line is a fit to the numerically calculated values and is given by

$$C(\alpha_o) = -1.28 + \alpha_o \frac{1 + 1.53\,\alpha_o}{0.18 + 0.76\,\alpha_o + 0.39\,\alpha_o^2}. \tag{3.9}$$

The dashed line corresponds to the asymptote as $\alpha_o \to \infty$. The circles represent the numerically calculated values. Equations (3.8) and (3.9) provide a fully analytic criterion for the critical Stokes number for particle–particle contact to occur. In many cases, this may also constitute the criterion for particle coagulation.

4. Summary and conclusions

This paper complements the previous work by Sundararajakumar & Koch (1996) on the energy dissipation due to lubrication flows during aerodynamic interparticle collisions. We have shown that collisions in a gas are qualitatively different from those occurring in liquids. Both the compressible and non-continuum nature of the gas need to be included in an accurate description of the collision process. Compressibility becomes important when the pressure drop between the particle surfaces (across the gap) becomes comparable to the atmospheric pressure. Non-continuum effects have to be included when the gap thickness is smaller than or comparable to the mean-free path of the bulk gas. The dimensionless parameter α_o characterizes the relative

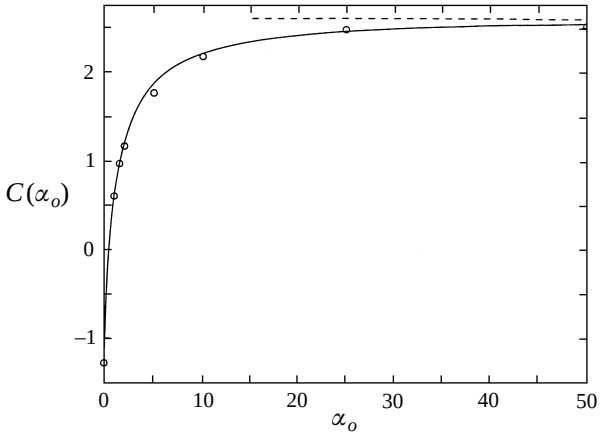

FIGURE 19. Figure showing $C(\alpha_o)$ given by (3.8) as a function of α_o. The dashed line is the asymptote corresponding to $\alpha_o = \infty$. The numerically calculated values are shown as circles.

importance of these two effects. A partial differential equation which incorporates both these effects is derived along with associated initial and boundary conditions.

In § 2, we considered collisions between particles characterized by large values of the Stokes number. Both compressibility and non-continuum effects on the dynamics of the collision process were studied separately as well as together. In the limit $St_o \to \infty$ the collision dynamics depends only on α_o. Expressions for the energy dissipated during the rebound and also the energy stored in the compressed gas were obtained from numerical results, cf. (2.19) and (2.20). These can be used to find the fractional energy loss due to viscous dissipation for large values of St_o, when the change in the particle velocities during the course of collision is small.

Collisions between equal-sized spheres characterized by finite values of St_o were then studied in § 3. In the presence of compressibility, the gas flow is not quasi-steady. The dynamics are found to depend on three parameters: α_o, St_o and the initial separation. When the Stokes number is very small, the behaviour is similar to that predicted by incompressible theory as was demonstrated (figure 14) for the particular case when $\alpha = \infty$. This observation however holds for all values of α_o as long as the Stokes number is small. As the Stokes number increases, compressibility effects become more important. In fact, for a certain range of St_o, the spheres are seen to rebound without actually coming into contact. This tendency to rebound vanishes in the limit $\alpha_o \to 0$ in which non-continuum effects dominate. A result for the minimum Stokes number, St_1, for actual contact to occur between the spheres, (3.9), was then derived. Whereas the primary effect of compressibility in a liquid is to cause rebound, the primary effect in a gas is to decrease the lubrication resistance and allow contact to occur, provided the particle Stokes number is sufficiently large. Thus, we find that contact is possible even without non-continuum effects.

In our analysis we neglected interparticle forces between the spheres. If we consider small particles with low inertia (for example particles with Stokes numbers slightly less than St_1), van der Waals attraction could lead to particle contact. Schmidt-Ott & Burtscher (1982) studied the effects of van der Waals forces on spherical aerosol particles and found that these are most effective in promoting coagulation between particles with radii of about 0.01 μm or less. For larger particles retardation effects were observed to decrease the enhancement factor. In the case of aerosol particles

with radii in the range 10–100 μm, the dispersion forces are expected to be small compared to the lubrication force and it seems likely that these forces play a part only after the viscous effects have almost brought the particles to a stop. It is thus expected that these forces will have a noticeable effect only in a small portion of the parameter space.

This work was supported by the US Environmental Protection Agency under grant number R81-9761-010.

REFERENCES

Alam, M. K. 1987 The effect of van der Waals and viscous forces on aerosol coagulation. *Aerosol Sci. Technol.* **6**, 41.

Barnocky, G. & Davis, R. H. 1989 The influence of pressure-dependent density and viscosity on the elastohydrodynamic collision and rebound of two spheres. *J. Fluid Mech.* **209**, 501.

Brazier-Smith, P. R., Jennings, S. G. & Latham, J. 1972 The interaction of falling water drops: coalescence. *Proc. R. Soc. Lond.* A **326**, 393.

Cercignani, C. & Daneri, A. 1963 Flow of a rarefied gas between two parallel plates. *J. Appl. Phys.* **34**, 3509.

Chang, M. B., Leong, K. H. & Stukel, J. J. 1987 Electrostatic and inertial collection of aerosol particles by water droplets. *Aerosol Sci. Technol.* **6**, 53.

Dahneke, B. J. 1973 Measurements of bouncing of small latex spheres. *J. Colloid. Interface Sci.* **45**, 584.

Davis, R. H., Serayssol, J.-M. & Hinch, E. J. 1986 The elastohydrodynamic collision of two spheres. *J. Fluid Mech.* **163**, 479.

Friedlander, S. K. 1977 *Smoke, Dust and Haze: Fundamentals of Aerosol Behavior*. Wiley.

Fuchs, N. A. 1964 *The Mechanics of Aerosols*. Pergamon.

Hidy, G. M. & Brock, J. R. 1970 *The Dynamics of Aerocolloidal Systems*. Pergamon.

Hocking, L. M. 1973 The effect of slip on the motion of a sphere close to a wall and of two adjacent spheres. *J. Engng Maths* **7**, 207.

Hocking, L. M. & Jonas, P. R. 1970 The collision efficiency of small drops. *Q. J. R. Met. Soc.* **96**, 722.

Jonas, P. R. & Goldsmith, P. 1972 The collection efficiencies of small droplets falling through a sheared air flow. *J. Fluid Mech.* **52**, 593.

Koch, D. L. 1990 Kinetic theory for a monodisperse gas–solid suspension. *Phys. Fluids* A **2**, 1711.

Kytömaa, H. K. & Schmid, P. J. 1992 On the collision of rigid spheres in a weakly compressible fluid. *Phys. Fluids* A **4**, 2683.

Leal, L. G. 1992 *Laminar Flow and Convective Transport Processes*. Butterworth–Heineman.

Lian, G., Adams, M. J. & Thornton, C. 1996 Elastohydrodynamic collisions of solid spheres. *J. Fluid Mech.* **311**, 141.

Mason, B. J. 1971 *The Physics of Clouds*. Oxford University Press.

Ochs, H. T. & Beard. K. V. 1985 Effects of coalescence efficiencies on the formation of precipitation. *J. Atmos. Sci.* **42**, 1451.

Pruppacher, H. R. & Klett, J. D. 1978 *Microphysics of Clouds and Precipitation*. Reidel.

Rogers, J. R. & Davis, R. H. 1990 The effects of van der Waals attractions on cloud droplet growth by coalescence. *J. Atmos. Sci.* **47**, 1075.

Schmidt-Ott, A. & Burtscher, H. 1982 The effect of van der Waals forces on aerosol coagulation. *J. Colloid Interface Sci.* **89**, 353.

Serayssol, J.-M. & Davis, R. H. 1986 The influence of surface interactions on the elastohydrodynamic collision of two spheres. *J. Colloid Interface Sci.* **114**, 54.

Spielman, L. A. 1970 Viscous interactions in Brownian coagulation. *J. Colloid Interface Sci.* **33**, 562.

Sundararajakumar, R. R. & Koch, D. L. 1996 Non–continuum flows between particles colliding in a gas. *J. Fluid Mech.* **313**, 283.

Twomey, S. 1977 *Atmospheric Aerosols*. Elsevier.

VERGELES, M., KEBLINSKI. P, KOPLIK, J. & BANAVAR, J. R. 1995 Stokes drag at the molecular level. *Phys. Rev. Lett*. **75**, 232.

WILLIAMS, M. M. R. & LOYALKA, S. K. 1991 *Aerosol Science Theory and Practice, with Special Applications to the Nuclear Industry*. Pergamon.

YING, R. & PETERS, M. H. 1989 Hydrodynamic interactions of two equal–sized spheres in a slightly rarefied gas: resistance and mobility functions. *J. Fluid Mech.* **207**, 353.

YING, R. & PETERS, M. H. 1991 Interparticle and particle-surface gas dynamic interactions. *Aerosol Sci. Technol.* **14**, 418